Journal of Magnetic Resonance 301 (2019) 49–55

Contents lists available at ScienceDirect

Journal of Magnetic Resonance

journal homepage: www.elsevier.com/locate/jmr

Homonuclear ADAPT: A general preparation route to long-lived nuclear singlet order

Stuart J. Elliott [a,1], Gabriele Stevanato [b,*]

[a] School of Chemistry, University of Southampton, Southampton SO17 1BJ, United Kingdom
[b] Institut des Sciences et Ingénierie Chimiques, Ecole Polytechnique Fédérale de Lausanne (EPFL), Batochime, CH-1015 Lausanne, Switzerland

ARTICLE INFO

Article history:
Received 26 October 2018
Revised 27 January 2019
Accepted 26 February 2019
Available online 4 March 2019

Keywords:
Long-lived state
Singlet order
ADAPT
SLIC
M2S
Sarkar sequence

ABSTRACT

We introduce a simple strategy to access and readout nuclear singlet order based on the alternate repetition of hard pulses and delays. We demonstrate the general applicability of the method by accessing nuclear singlet order in spin systems characterized by diverse coupling regimes. We show that the method is highly efficient in the strong-coupling and chemical equivalence regimes, and can overcome some limitations of other well-established and more elaborated pulse sequences. A simulation package is provided which allows the determination of pulse sequence parameters.

1. Introduction

Nuclear magnetic resonance (NMR) experiments are restricted by the relaxation of longitudinal magnetization in solution, which decays with the characteristic time constant T_1. Long-lived states (LLS) offer a promising means to alleviate this limitation [1–15]. In pairs of spin-1/2 homonuclei, the LLS is unaffected by in pair dipole-dipole relaxation and showcases extended lifetimes with respect to T_1. The LLS is defined as the imbalance between the population of the exchange-antisymmetric nuclear singlet state and the mean population of the exchange-symmetric nuclear triplet states (referred to as nuclear singlet order) and has a relaxation time constant denoted T_S.

Since the first successful demonstration of LLS [1], an increasing effort has been devoted to: the extension of LLS lifetimes in strongly-coupled spin systems [16], LLS in multi-spin environments such as methyl groups [17–24], and the theoretical elucidation of the principle mechanisms responsible for LLS relaxation [25–28]. These developments lead to the synthesis of a $^{13}C_2$-naphthalene derivative with a LLS lifetime exceeding one hour in room temperature solution [29–31]. Proof of principle experiments to image the prolonged lifetime of singlet order have also been demonstrated [32,33]. Other important applications include: the contrast enhancement provided by LLS for protein-ligand binding interactions [34–36], drug screening using hyperpolarized LLS [37], nuclear singlet multimers (NUSIMERs) [38], and the introduction of a singlet tag (STAG) that can be incorporated into a number of biomolecules [39].

Preparation and detection of LLS requires the following steps: (i) excitation: longitudinal magnetization is converted into a long-lived population imbalance; (ii) evolution: the long-lived order evolves during a free evolution delay τ_{ev}; (iii) conversion: the evolved state is transformed into detectable magnetization. LLS are typically prepared by using the M2S [40,41], SLIC [42] and Sarkar [43] pulse sequences, and their variants [44–46], depending on the coupling regime between the participating homonuclei. A comprehensive and detailed description of the current methods has also been published [47]. Access to LLS is provided by small differences in chemical shift or asymmetric J-couplings to magnetic nuclei outside of the singlet pair [9,40–42,48,49]. The individual methods are ultimately restricted to a distinct coupling regime, i.e. SLIC and M2S sequences are employed under strong-coupling and chemical equivalence conditions, and the Sarkar method is used for weakly-coupled systems.

Here we propose an adaptable method based on a repeated module of a single hard pulse and a delay. The pulse sequence

* Corresponding author.
E-mail address: gabriele.stevanato@epfl.ch (G. Stevanato).
[1] Current address: Centre de Resonance Magnétique Nucléaire à Très Hauts Champs de Lyon – FRE 2034 CNRS/Université Claude Bernard Lyon 1/ENS de Lyon, Institut des Sciences Analytiques – UMR 5280, 5 Rue de la Doua, Université de Lyon, 69100 Villeurbanne, France

https://doi.org/10.1016/j.jmr.2019.02.005
1090-7807/

can be used to generate LLS for pairs of spin-1/2 nuclei characterized by a diverse range of coupling regimes. Experimental demonstrations are presented for the cases of a ^{13}C labelled naphthalene derivative ($^{13}C_2$-**I**), 1-^{13}C labelled disodium fumarate (^{13}C-**II**) and the dipeptide alanine-glycine (Ala-Gly), see Fig. 2a, c and e, respectively. The pulse sequence is flexible with respect to the use of small or large flip angle pulses. The delay between hard pulses and the number of repetitions is simple to optimize, and can be predicted in the strong-coupling and chemical equivalence limits or simulated based on prior knowledge of the spin pair J-coupling and chemical shift difference. The pulse sequence is highly efficient and rapidly interconverts transverse magnetization and singlet order under strong-coupling and chemical equivalence conditions. A refocused variant of the ADAPT sequence is also demonstrated, and performs well in the strong-coupling limit. Since a similar strategy has recently been implemented to achieve heteronuclear polarization transfer in PHIP and SABRE experiments [50,51], we name the sequence *homonuclear* ADAPT. We provide a custom-made *SpinDynamica* code that simulates the pulse sequence for a pair of spins experiencing any coupling regime [52].

2. Pulse sequence

For a homonuclear spin-1/2 pair, a suitable basis set $X = \{|1\rangle, |2\rangle, |3\rangle, |4\rangle\}$ is the simultaneous eigenbasis of the operators $I_1 \cdot I_2$ and I_x:

$$\begin{aligned} |1\rangle &= \tfrac{|\beta\beta\rangle}{2} - \tfrac{|\beta\alpha\rangle}{2} - \tfrac{|\alpha\beta\rangle}{2} + \tfrac{|\alpha\alpha\rangle}{2} \\ |2\rangle &= \tfrac{|\beta\beta\rangle}{2} + \tfrac{|\beta\alpha\rangle}{2} + \tfrac{|\alpha\beta\rangle}{2} + \tfrac{|\alpha\alpha\rangle}{2} \\ |3\rangle &= \tfrac{|\beta\beta\rangle}{\sqrt{2}} - \tfrac{|\alpha\alpha\rangle}{\sqrt{2}} \\ |4\rangle &= \tfrac{|\alpha\beta\rangle}{\sqrt{2}} - \tfrac{|\beta\alpha\rangle}{\sqrt{2}} \end{aligned} \quad (1)$$

using standard Dirac notation. The initial equilibrium state is proportional to longitudinal Zeeman order $\rho_① = I_z$, where ⑪ is the time point defined in Fig. 1. The initial 90$_y$ pulse converts I_z into transverse magnetization I_x. In the adopted basis set, the matrix representation of $\rho_② = I_x$ contains elements along the diagonal and is written as:

$$\rho_② = I_x \propto -(|1\rangle\langle 1| - |2\rangle\langle 2|) \quad (2)$$

The effect of the ADAPT sequence is to produce an approximate π rotation in the subspace spanned by the vectors $|1\rangle$ and $|4\rangle$, whilst leaving the population of the state $|2\rangle$ approximately unperturbed. $\rho_③$ is consequently expressed by the population imbalance:

$$\rho_③ \propto -(|4\rangle\langle 4| - |2\rangle\langle 2|) \quad (3)$$

By recognizing that $|2\rangle = (|T_{-1}\rangle/2 + |T_0\rangle/\sqrt{2} + |T_{+1}\rangle/2)$ and $|4\rangle = |S_0\rangle$, it becomes apparent that the ADAPT method accesses the homonuclear population imbalance between the singlet and triplet manifolds.

The parameters Δ_α and m_α of the *homonuclear* ADAPT cycle are chosen to maximise triplet-singlet population conversion for a given α. In the strong coupling regime (as shown in Eqs. (S22) and (S23)):

$$\Delta_\alpha = \frac{\alpha}{\omega_{\text{eff}}} \quad (4)$$

$$m_\alpha = \text{Round}\left[\frac{\pi}{2\arccos\left(\frac{1}{2}(1+\cos(\alpha)+\cos(\theta)-\cos(\alpha)\cos(\theta))\right)}\right] \quad (5)$$

with ω_{eff} and θ (defined in Eq. S8) related to the effective precession frequency and the degree of chemical inequivalence between homonuclei.

The inverse of Δ_α is proportional to the effective nutation frequency ω_{eff} defined in S8. In the magnetic equivalence limit, ω_{eff} approaches the value of the homonuclear J coupling. The total duration of the sequence for any tip angle is proportional to $1/\omega_\Delta$ with ω_Δ (see S8) being the degree of magnetic inequivalence in the spin system. Intuitively, there is a close analogy between homonuclear ADAPT and the Spin Lock Induced Crossing (SLIC) sequence [42].

CW irradiation may be applied to sustain the population imbalance $\rho_③$, minimizing coherent relaxation effects induced by the chemical shift difference $\omega_\Delta/2\pi$ [26]. At this point, it is possible that the density operator $\rho_④$ may include terms other than singlet order. T_{00} filtration may be used to select solely the long-lived component $\rho_⑤$ [21,53,54], which is subsequently reconverted to transverse magnetization for detection: $\rho_⑥ = I_x$. For further details, including advantages and disadvantages of the ADAPT pulse sequence, see the Electronic Supporting Information (ESI).

3. Results and discussion

We selected $\alpha = 18^\circ$ and $\alpha = 90^\circ$ as representative cases for small and large ADAPT pulse flip angles, respectively. The choice of $\alpha \neq \pi$ is arbitrary and when combined with the appropriate Δ_α the ADAPT sequence can perform magnetization to singlet order conversion. The different coupling regimes are presented below.

3.1. The strong-coupling limit: $^{13}C_2$-**I**

Two spin-1/2 nuclei are strongly-coupled in the case that the homonuclear J-coupling exceeds the isotropic chemical shift difference: $\omega_J \gg \omega_\Delta$. This is the case for the two central ^{13}C nuclei of $^{13}C_2$-**I**, see Fig. 2a. The relevant part of the experimental ^{13}C NMR spectrum of $^{13}C_2$-**I** is shown in Fig. 2b. The spectrum is consistent with a J-coupling of $\omega_J/2\pi = 54.6 \pm 0.2$ Hz and a chemical shift difference of $\omega_\Delta/2\pi = 12.8 \pm 0.1$ Hz between the ^{13}C sites, as reported previously [30].

Experimental results and numerical simulations demonstrating the transfer of $^{13}C_2$-**I** magnetization to singlet order under the ADAPT$_{18}$ sequence are shown in Fig. 3a and b, respectively. The integrals of the singlet-filtered data points were normalized relative to the NMR signal amplitude induced by a single 90° pulse. An optimal transfer efficiency of 39.9% is obtained by using m_{18} = 53 and Δ_{18} = 0.9 ms. Details of ADAPT$_{90}$ pulse sequence optimization are shown in the Electronic Supporting Information (ESI). The agreement of experimental results with numerical simulations is adequate, except for a noticeable loss in experimental conversion efficiency relative to the theoretical maximum of ~2/3 [55–57], which is associated with radiofrequency field imperfections and relaxation. A small deviation between theoretical and experimental loop numbers is also observed. One tentative explanation for the discrepancy could be imperfections regarding the initial 90° pulse duration calibration. The cumulative error introduced by multiple ADAPT cycles could be conducive to the mismatch between simulated and experimental results. The experimental dependence of the ADAPT$_{18}$ singlet-triplet transfer on the hard pulse flip angle is shown in the Electronic Supporting Information (ESI). In addition, off-resonance contributions to the spin system evolution were not considered in the simulations. Despite the relevance of these details, we did not investigate this issue further.

We implemented the SLIC and M2S pulse sequences to determine the singlet lifetime T_S as a benchmark for the performance of the ADAPT pulsed method. The SLIC and M2S experimental optimization protocol has previously been described elsewhere [40–42]. The SLIC and M2S pulse sequences used the parameters detailed in Table 1.

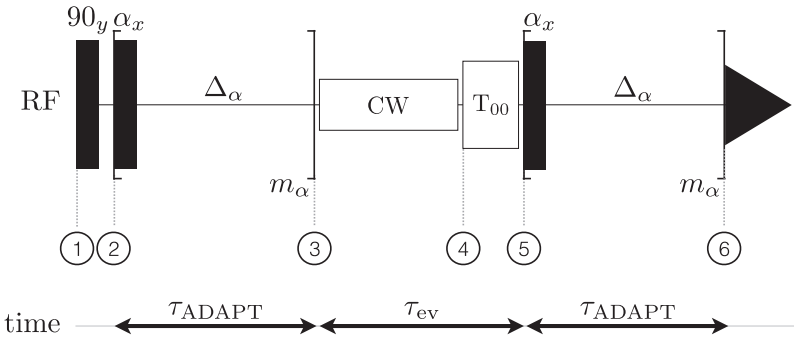

Fig. 1. Sequence of radiofrequency events used to convert, and subsequently reconvert, observable magnetization into singlet order, and measure the LLS lifetime T_S. τ_{ADAPT} indicates the duration of the ADAPT excitation and conversion blocks, with $\tau_{ADAPT} \simeq m_\alpha \times \Delta_\alpha$. Singlet order is allowed to evolve for a time τ_{ev}. On resonant continuous wave (CW) rf-irradiation may be applied to impose strong-coupling during τ_{ev}. The T_{00} filter, described in Refs. [21,53,54] and the ESI, retains only singlet order at the end of τ_{ev}. The variable evolution delay τ_{ev} is incremented to monitor the decay of singlet order. ⓝ denotes the time point at which the spin density operator is evaluated.

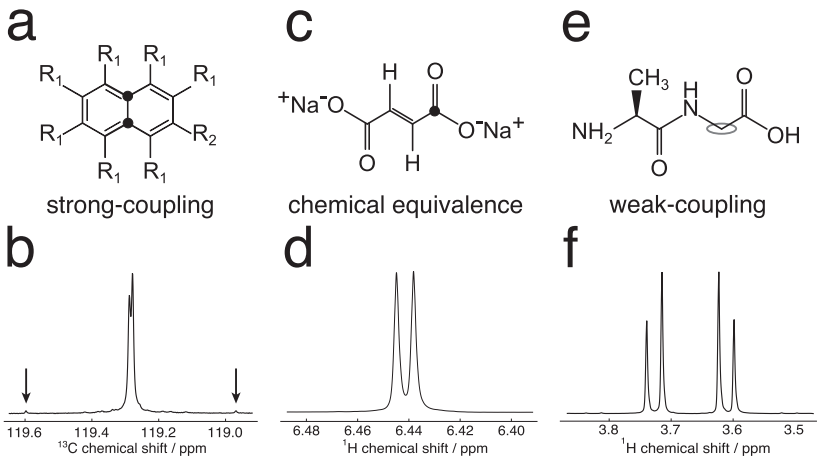

Fig. 2. (a) Molecular structure of the naphthalene derivative $^{13}C_2$-**I**. Black filled circles denote the ^{13}C labelling sites. $R_1 = CD_3$, $R_2 = CD(CD_3)_2$. (b) Relevant part of the experimental ^{13}C NMR spectrum of 0.2 M $^{13}C_2$-**I** in degassed tert-butanol-d_{10} solvent acquired at 16.45 T (176 MHz) with 16 transients (for the full ^{13}C spectrum, see the ESI). The small outer components of the AB spectral pattern are indicated by arrows. (c) Molecular structure of ^{13}C labelled disodium fumarate. (d) Relevant portion of the experimental ^{1}H NMR spectrum of 0.37 M ^{13}C-**II** in degassed D_2O solution acquired at 16.45 T (700 MHz) with a single transient (for the full ^{1}H spectrum, see the ESI). (e) Molecular structure of the dipeptide Ala-Gly. The pair of protons participating in the LLS is circled in grey. (f) CH_2 portion of the experimental ^{1}H NMR spectrum of 0.1 M Ala-Gly in degassed D_2O solution acquired at 16.45 T (700 MHz) with 2 transients (for the full ^{1}H spectrum, see the ESI). (For interpretation of the references to colour in this figure legend, the reader is referred to the web version of this article.)

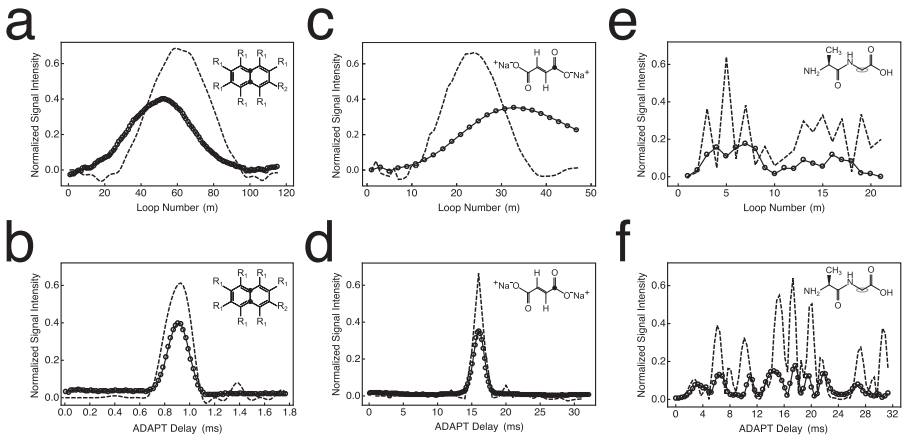

Fig. 3. Conversion amplitudes for the transfer of transverse magnetization to singlet order for (a,b) 0.2 M $^{13}C_2$-**I** in degassed tert-butanol-d_{10} solvent, (c,d) 0.37 M ^{13}C-**II** in degassed D_2O solution and (e,f)* 0.1 M Ala-Gly in degassed D_2O solution using the pulse sequence shown in Fig. 1. Experiments were performed at 16.45 T (^{1}H Larmor frequency = 700 MHz, ^{13}C Larmor frequency = 176 MHz) and 25°C with two transients per data point. Experimental data: black open circles; simulations: black dashed lines. The signal intensity is normalized such that 1.0 corresponds to the thermal equilibrium signal intensity. The maximum simulated signal intensity is 2/3. The optimal conversion efficiency was 39.9% for $^{13}C_2$-**I**, 35.2% for ^{13}C-**II** and 17.7% for Ala-Gly. The delay between successive experiments is 65 s for $^{13}C_2$-**I**, 175 s for ^{13}C-**II** and 125 s for Ala-Gly. (a) Optimization of $ADAPT_{18}$ loop number for $^{13}C_2$-**I** with Δ_{18} fixed at 0.9 ms. (b) Optimization of $ADAPT_{18}$ delay for $^{13}C_2$-**I** with m_{18} fixed at 53. (c) Optimization of $ADAPT_{90}$ loop number for ^{13}C-**II** with Δ_{90} fixed at 16.0 ms. (d) Optimization of $ADAPT_{90}$ delay for ^{13}C-**II** with m_{90} fixed at 33. (e) Optimization of $ADAPT_{90}$ loop number for Ala-Gly with Δ_{90} fixed at 17.9 ms. (f) Optimization of $ADAPT_{90}$ delay for Ala-Gly with m_{90} fixed at 7. *Absolute value of the normalized signal intensity plotted.

Table 1
Experimental conversion efficiencies (ϵ), durations (D), parameters and singlet lifetimes (T_S) for $^{13}C_2$-**I** obtained by using the ADAPT$_{18}$, ADAPT$_{90}$, SLIC and M2S pulse sequences.

$^{13}C_2$-**I**	ϵ/%	D/ms	Δ_α/ms	m_α	ν_{SL}/Hz	τ_{SL}/ms	Δ/ms	n_1	n_2	T_S/s
ADAPT$_{18}$	39.9	54.9	0.9	61	–	–	–	–	–	13.07 ± 0.03
ADAPT$_{90}$	34.1	58.5	4.5	13	–	–	–	–	–	13.12 ± 0.05
SLIC	39.4	55.1	–	–	54.6	55.1	–	–	–	13.17 ± 0.03
M2S	35.1	88.7	–	–	–	–	4.66	6	3	13.31 ± 0.06

The M2S sequence takes 88.7 ms to achieve singlet-triplet interconversion using optimized experimental conditions, a factor of $\sim 2/\pi$ longer than the ADAPT$_{18}$ and SLIC methods, see Table 1. The efficiencies of the SLIC and M2S sequences were estimated from spectral integration as 39.4% and 35.1%, respectively. The SLIC pulse conversion efficiency was found to be remarkably similar to that of the ADAPT$_{18}$ sequence. A comparison of the offset dependence for the ADAPT$_{18}$, SLIC and M2S pulse sequences is given in the Electronic Supporting Information (ESI), in conjunction with a refocused ADAPT sequence which achieves broadband singlet-triplet conversion.

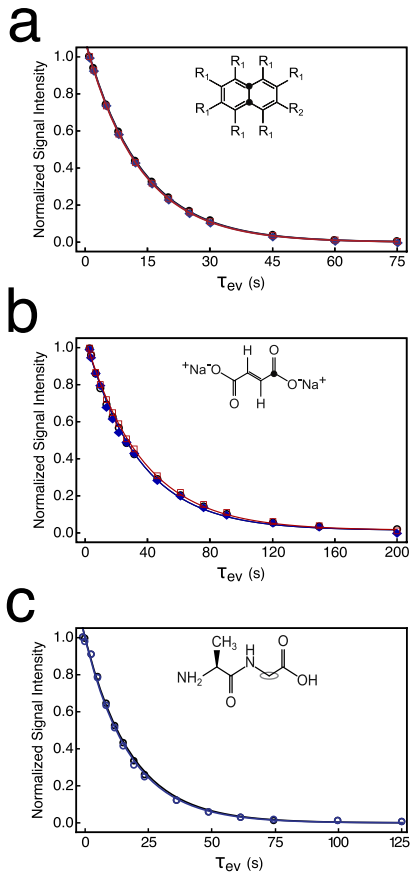

Fig. 4. Experimental relaxation curves for (a) 0.2 M $^{13}C_2$-**I** in degassed tert-butanol-d_{10} solvent, (b) 0.37 M ^{13}C-**II** in degassed D_2O solution and (c) 0.1 M Ala-Gly in degassed D_2O solution. Experiments were performed at 16.45 T (^{1}H Larmor frequency = 700 MHz, ^{13}C Larmor frequency = 176 MHz) and 25°C with two transients per data point. Decays curves were obtained by implementing the following pulse sequences: (a) ADAPT$_{18}$ (red open squares), SLIC (blue filled diamonds), M2S (black open circles); (b) ADAPT$_{90}$ (red open squares), SLIC (blue filled diamonds), M2S (black open circles); (c) ADAPT$_{90}$ (blue open circles), Sarkar sequence (black open circles). All signal amplitudes were normalized with respect to the first data point. All fitted curves have a single exponential form. The delay between successive experiments is 65 s for $^{13}C_2$-**I**, 175 s for ^{13}C-**II** and 125 s for Ala-Gly. CW irradiation (nutation frequency = 3 kHz) was used to sustain the LLS of Ala-Gly during the evolution delay τ_{ev}. (For interpretation of the references to colour in this figure legend, the reader is referred to the web version of this article.)

The singlet lifetime of $^{13}C_2$-**I** was estimated by using the ADAPT$_{18}$ pulse sequence, see Fig. 4a (red curve). This shows a single exponential decay with a singlet relaxation time constant T_S = 13.07 ± 0.03 s. The spin-lattice relaxation time was estimated from a separate inversion-recovery experiment to be T_1 = 686 ± 4 ms. The ADAPT$_{90}$ pulse sequence was also used to estimate the singlet lifetime, returning T_S = 13.12 ± 0.05 s.

Fig. 4a denotes the decay of singlet order measured by implementing the SLIC (blue curve) and M2S (black curve) pulse sequences. The two curves have the following time constants: SLIC: T_S = 13.17 ± 0.03 s; M2S: T_S = 13.31 ± 0.06 s. These values are in good agreement with the values of T_S determined by using the ADAPT$_{18}$ and ADAPT$_{90}$ pulse sequences.

As demonstrated in Fig. S9 of the Electronic Supporting Information (ESI), different ADAPT schemes for excitation and reconversion of singlet order can additionally be used.

3.2. The chemical equivalence limit: ^{13}C-*II*

The constituents of a spin-1/2 pair are chemically equivalent in the case that the chemical shift difference between the two sites is zero: $\omega_\Delta = 0$. This is the case for the two *trans*-protons of ^{13}C-**II**, see Fig. 2c. The relevant region of the experimental ^{1}H NMR spectrum of ^{13}C-**II** is shown in Fig. 2d. The spectrum corresponds to a chemically equivalent proton pair with the following J-coupling network: $\omega_{J_{H1H2}}/2\pi = 15.7 \pm 0.4$ Hz; $\omega_{\Sigma J}/2\pi = J_{H1C} + J_{H2C}$ = 10.0 ± 0.3 Hz; $\omega_{\Delta J}/2\pi = J_{H1C} - J_{H2C}$ = 4.2 ± 0.2 Hz.

Results illustrating the ADAPT$_{90}$-mediated transfer of ^{13}C-**II** magnetization to singlet order are presented in Fig. 3c and d. A maximal conversion efficiency of 35.2% is obtained by using an ADAPT$_{90}$ loop number m_{90} = 33 and delay time Δ_{90} = 16.0 ms. The agreement between experimental results and numerical simulations is satisfactory. The experimental parameters and conversion efficiency determined from the optimization of the ADAPT$_{18}$ method are shown in Table 2.

It has previously been demonstrated that singlet order conversion methods which work well in the strong-coupling regime can also be implemented in the chemical equivalence limit [9,48,49,58]. For the case of ^{13}C-**II**, the SLIC and M2S pulse sequence parameters are given in Table 2. The total duration of the M2S sequence is considerably longer than the ADAPT$_{18}$ and SLIC techniques.

The singlet lifetime of ^{13}C-**II** was measured by using the ADAPT$_{90}$ conversion sequence, Fig. 4b (red curve). This shows a single exponential decay with a singlet relaxation time constant T_S = 36.7 ± 0.7 s. The longitudinal relaxation time was estimated from a separate inversion-recovery experiment to be T_1 = 33.3 ± 0.5 s. The ADAPT$_{18}$ pulse sequence is additionally employed to track the decay of nuclear singlet order, yielding T_S = 36.8 ± 0.5 s.

The blue and black curves in Fig. 4b highlight the decay of proton singlet order measured by using the SLIC and M2S pulsed methods, respectively. The two curves have the following time constants: SLIC: T_S = 34.8 ± 0.7 s; M2S: T_S = 34.8 ± 0.7 s. These values are in good agreement with the values of T_S estimated by using the ADAPT$_{90}$ and ADAPT$_{18}$ pulse sequences.

Table 2
Experimental conversion efficiencies (ϵ), durations (D), parameters and singlet lifetimes (T_S) for ^{13}C-**II** obtained by using the ADAPT$_{90}$, ADAPT$_{18}$, SLIC and M2S pulse sequences.

^{13}C-**II**	ϵ/%	D/ms	Δ_α/ms	m_α	ν_{SL}/Hz	τ_{SL}/ms	Δ/ms	n_1	n_2	T_S/s
ADAPT$_{90}$	35.2	342.0	3.2	106	–	–	–	–	–	36.7 ± 0.7
ADAPT$_{18}$	36.2	384.0	16.0	24	–	–	–	–	–	36.8 ± 0.5
SLIC	49.2	332.7	–	–	15.7	332.7	–	–	–	34.8 ± 0.7
M2S	47.0	697.8	–	–	–	–	15.8	14	7	34.8 ± 0.5

As demonstrated in Fig. S10 of the Electronic Supporting Information (ESI), different ADAPT schemes for excitation and reconversion of singlet order can be used.

3.3. The weak-coupling limit: Ala-Gly

Two spin-1/2 nuclei are weakly-coupled in the case that the homonuclear J-coupling is smaller than the isotropic chemical shift difference: $\omega_J \ll \omega_\Delta$. This is the case for the two vicinal protons of Ala-Gly, see Fig. 2e. The CH_2 portion of the experimental ^{1}H NMR spectrum of Ala-Gly is shown in Fig. 2f. The spectrum is consistent with the following parameters: $\omega_J/2\pi = 17.2 \pm 0.1$ Hz and $\omega_\Delta/2\pi = 79.8 \pm 0.4$ Hz. These parameters are consistent with the literature [59].

A relevant distinction between strong- and weak-coupling regimes is the singlet precursor state. In the strong-coupling regime, singlet order is close to an exact eigenstate of the spin Hamiltonian. The singlet and central triplet states represent two approximately disconnected eigenstates, linked only by a small difference in isotropic chemical shift. As a result, the precursor state populated at the end of a singlet excitation scheme is long-lived without intervention from rf-fields or sample shuttling to low field [26,40,60]. However, the singlet precursor state in a weakly-coupled system is far from an approximate eigenstate of the spin Hamiltonian, and does not directly correspond to well-defined singlet order as the large chemical shift difference causes strong mixing between the singlet and triplet states. The precursor state populated after a singlet excitation sequence is projected onto singlet order by externally applied CW fields used to sustain the long-lived spin order during evolution intervals.

Results demonstrating the transfer of proton magnetization to singlet order under the ADAPT$_{90}$ sequence are reported in Fig. 3e and f. An optimal transfer efficiency of 17.7% is obtained by using an ADAPT$_{90}$ loop number of $m_{90} = 7$, although an ADAPT$_{90}$ loop number between $m = 3$ and $m = 8$ achieves >10% triplet-singlet conversion efficiency, and an inter-delay of $\Delta_{90} = 17.9$ ms, with other efficient delay periods also permissible. The experimental results are in adequate agreement with the numerical simulations.

A CW field amplitude of 3 kHz was used to sustain the LLS of Ala-Gly during the evolution period τ_{ev}. A relaxation curve for proton singlet order is shown in Fig. 4c (blue curve). This shows a monoexponential decay with time constant $T_S = 21.0 \pm 0.6$ s. The experimental time constant is in agreement with previous singlet lifetime measurements on this polypeptide [59]. The longitudinal relaxation time was estimated from a separate inversion-recovery experiment to be $T_1 = 1.57 \pm 0.01$ s. The decay of proton singlet order was additionally tracked by using the ADAPT$_{18}$ pulse sequence, see the Electronic Supporting Information (ESI) for more details. A single exponential decay curve was observed, with singlet relaxation time constant $T_S = 20.0 \pm 0.4$ s. The two measurements are within experimental error.

The Sarkar sequence [43] is a well-known and efficient strategy to access LLS in the weak-coupling regime. The Sarkar sequence was consequently chosen as a comparative method for the measurement of T_S in weakly-coupled systems. The timings and conversion efficiency of the Sarkar sequence are given in Table 3.

The black curve in Fig. 4c corresponds to the decay of proton singlet order measured by using the Sarkar sequence. The monoexponential decay has the following singlet relaxation time: $T_S = 21.6 \pm 0.6$ s. The experimental decay time is in excellent agreement with the singlet lifetimes measured by the ADAPT$_{18}$ and ADAPT$_{90}$ methods.

Contrasting ADAPT cycles may be implemented to excite and reconvert proton singlet order of Ala-Gly as demonstrated in Fig. S11 the Electronic Supporting Information (ESI).

4. Numerical simulations using SpinDynamica

As demonstrated in Section 3.3, the applicability of the ADAPT pulse sequence is not solely limited to systems in the strong-coupling and chemical equivalence limits. For weakly-coupled spin pairs, an analytical treatment such as the analysis developed in the Electronic Supporting Information (ESI) is neither obvious nor straightforward. In this case, a more reasonable and faster approach would be to implement a numerical routine that is simple to use and can be modified according to specific user needs in order to determine the optimum ADAPT sequence parameters Δ_α and m_α.

A short numerical code suitable for these purposes is given in the Electronic Supporting Information (ESI). The *SpinDynamica* [52] routine simulates the effects of the pulse sequence in Fig. 1 to the end the first ADAPT cycle, i.e. the transformation of transverse magnetization to singlet order. The code produces a 2D contour plot as a function of the ADAPT delay Δ_α and the loop number m_α, see Fig. 5. Bright yellow regions indicate optimal values of Δ_α and m_α, and provide a straightforward indication of the relevant parameter space to search experimentally.

A numerical simulation of the ADAPT$_{18}$ sequence for $^{13}C_2$-**I** returns $\Delta_{18} = 0.9$ ms and $m_{18} = 61$, see Fig. 5a. These values are in good agreement with the experimental data, see Fig. 3a and b, and the parameters predicted by the analytical formalization, see the Electronic Supporting Information (ESI). Fig. 5b reports a numerical simulation for Ala-Gly using the ADAPT$_{90}$ pulse sequence. The simulation computed the following parameters: $\Delta_{90} = 17.2$ ms and $m_{90} = 5$. These values are in approximate agreement with the experimentally determined parameters although a

Table 3
Experimental conversion efficiencies (ϵ), durations (D), parameters and singlet lifetimes (T_S) for Ala-Gly obtained by using the ADAPT$_{90}$, ADAPT$_{18}$ and Sarkar pulse sequences.

Ala-Gly	ϵ/%	D/ms	Δ_α/ms	m_α	τ_1/ms	τ_2/ms	T_S/s
ADAPT$_{90}$	17.7	86.0	17.2	5	–	–	21.0 ± 0.6
ADAPT$_{18}$	6.8	127.2	21.2	6	–	–	20.0 ± 0.4
Sarkar	11.0	35.3	–	–	14.5	6.3	21.6 ± 0.6

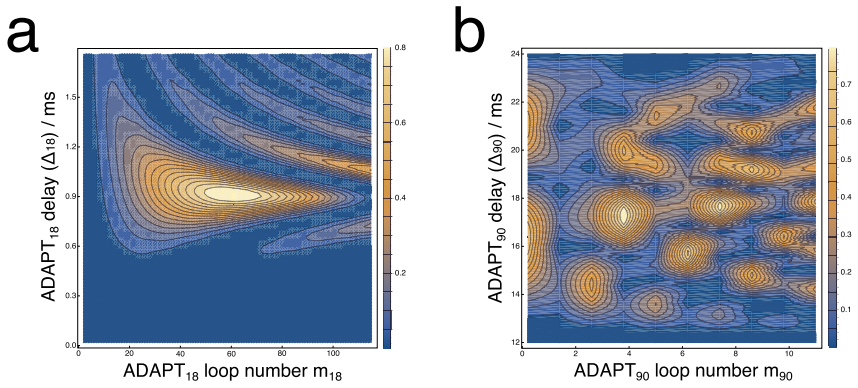

Fig. 5. Simulated 2D contour plots of homonuclear ADAPT transfers for (a) $^{13}C_2$-**I** and (b) Ala-Gly. Longitudinal magnetization is converted to singlet order under the action of the coherent spin Hamiltonian given in Eq. (S1). The experimental parameters for $^{13}C_2$-**I** and Ala-Gly are given in Section 3. No relaxation was included in the simulations.

discrepancy remains, see Fig. 3c and d. Numerical trajectories detailing the conversion of magnetization to singlet order are presented in the Electronic Supporting Information (ESI).

5. Conclusions

We have conceived an alternative pulse sequence to access long-lived singlet order based on a repeated pulse-delay module. The *homonuclear* ADAPT method has been experimentally validated for a large range of coupling regimes, and has been compared against commonly used long-lived state preparation procedures. The sequence efficiently converts magnetization to singlet order in the strong-coupling and chemical equivalence regimes. A refocused *homonuclear* ADAPT sequence, demonstrated in the strong-coupling limit, overcomes issues related to spin system evolution under a resonance offset, making the sequence general and robust. Analytical expressions for the delay Δ_α and the number of loops m_α have been derived under strong-coupling and chemical equivalence conditions, and are in good agreement with the experimentally determined parameters. A custom-made *SpinDynamica*-based routine is provided to numerically calculate the delay between hard pulses and the number of loops. As the pulse sequence is easy to implement and flexible with respect to the hard pulse flip angle, we believe that the *homonuclear* ADAPT is a promising method for use in the future applications of long-lived states.

Acknowledgements

This research was supported by the Engineering and Physical Sciences Research Council (EPSRC) UK, grant code EP/L505067/1, ERC (advanced grant N. 320860), the Marie-Skłodowska-Curie program of the European Community (796904-Oligo-DNP) and Bruker BioSpin UK. The authors gratefully acknowledge Malcolm H. Levitt and Lyndon Emsley for support, guidance and encouragement, Christian Bengs for carefully reading the manuscript prior to publication, Giuseppe Pileio and Stefan Glöggler for enlightening discussions, Lynda J. Brown for synthesis of $^{13}C_2$-**I**, and Sally Bloodworth, James Eills and Aliki Moysiadi for sample preparation.

Appendix A. Supplementary material

Supplementary data associated with this article can be found, in the online version, at https://doi.org/10.1016/j.jmr.2019.02.005.

References

[1] M. Carravetta, O. Johannessen, M. Levitt, Phys. Rev. Lett. 92 (2004) 153003.
[2] G. Pileio, M.H. Levitt, J. Magn. Reson. 187 (2007) 141–145.
[3] G. Pileio, M. Carravetta, E. Hughes, M.H. Levitt, J. Am. Chem. Soc. 130 (2008) 12582–12583.
[4] P.R. Vasos, A. Comment, R. Sarkar, P. Ahuja, S. Jannin, J.-P. Ansermet, J.A. Konter, P. Hautle, B. van den Brandt, G. Bodenhausen, Proc. Natl. Acad. Sci. USA 106 (2009) 18469–18473.
[5] M.C.D. Tayler, I. Marco-Rius, M.I. Kettunen, K.M. Brindle, M.H. Levitt, G. Pileio, J. Am. Chem. Soc. 134 (2012) 7668–7671.
[6] M.H. Levitt, Annu. Rev. Phys. Chem. 63 (2012) 89–105.
[7] G. Pileio, S. Bowen, C. Laustsen, M.C.D. Tayler, J.T. Hill-Cousins, L.J. Brown, R.C. D. Brown, J.-H. Ardenkjaer-Larsen, M.H. Levitt, J. Am. Chem. Soc. 135 (2013) 5084–5088.
[8] Y. Feng, T. Theis, X. Liang, Q. Wang, P. Zhou, W.S. Warren, J. Am. Chem. Soc. 135 (2013) 9632–9635.
[9] K. Claytor, T. Theis, Y. Feng, W. Warren, J. Magn. Reson. 239 (2014) 81–86.
[10] S.J. Elliott, P. Kadeřávek, L.J. Brown, M. Sabba, S. Glöggler, D.J. O'Leary, R.C.D. Brown, F. Ferrage, M.H. Levitt, Mol. Phys. 0 (2018) 1–7.
[11] B.A. Rodin, K.F. Sheberstov, A.S. Kiryutin, J.T. Hill-Cousins, L.J. Brown, R.C.D. Brown, B. Jamain, H. Zimmermann, R.Z. Sagdeev, A.V. Yurkovskaya, K.L. Ivanov, ArXiV, 2018, 1810.12697.
[12] S. Mamone, S. Glöggler, Phys. Chem. Chem. Phys. 20 (2018) 22463–22467.
[13] A.S. Kiryutin, M.S. Panov, A.V. Yurkovskaya, K.L. Ivanov, G. Bodenhausen, ChemPhysChem 0 (2019) 1–7.
[14] S. Glöggler, S. Yang, J. McCormick, S. Mamone, L.-S. Bouchard, Angew. Chem. Int. Ed. (2019).
[15] B.B. Kharkov, X. Duan, E.S. Tovar, J.W. Canary, A. Jerschow, Phys. Chem. Chem. Phys. (2019).
[16] G. Pileio, J.T. Hill-Cousins, S. Mitchell, I. Kuprov, L.J. Brown, R.C.D. Brown, M.H. Levitt, J. Am. Chem. Soc. 134 (2012) 17494–17497.
[17] B. Meier, J.-N. Dumez, G. Stevanato, J.T. Hill-Cousins, S.S. Roy, P. Håkansson, S. Mamone, R.C.D. Brown, G. Pileio, M.H. Levitt, J. Am. Chem. Soc. 135 (2013) 18746–18749.
[18] J.-N. Dumez, P. Håkansson, S. Mamone, B. Meier, G. Stevanato, J.T. Hill-Cousins, S.S. Roy, R.C.D. Brown, G. Pileio, M.H. Levitt, J. Chem. Phys. 142 (2015) 044506.
[19] S.S. Roy, J.-N. Dumez, G. Stevanato, B. Meier, J.T. Hill-Cousins, R.C. Brown, G. Pileio, M.H. Levitt, J. Magn. Reson. 250 (2015) 25–28.
[20] G. Stevanato, S.S. Roy, J. Hill-Cousins, I. Kuprov, L.J. Brown, R.C.D. Brown, G. Pileio, M.H. Levitt, Phys. Chem. Chem. Phys. 17 (2015) 5913–5922.
[21] S.J. Elliott, L.J. Brown, J.-N. Dumez, M.H. Levitt, Phys. Chem. Chem. Phys. 18 (2016) 17965–17972.
[22] S.J. Elliott, L.J. Brown, J.-N. Dumez, M.H. Levitt, J. Magn. Reson. 272 (2016) 87–90.
[23] A. Jhajharia, E.M.M. Weber, J.G. Kempf, D. Abergel, G. Bodenhausen, D. Kurzbach, J. Chem. Phys. 146 (2017) 041101.
[24] S.J. Elliott, B. Meier, B. Vuichoud, G. Stevanato, L.J. Brown, J. Alonso-Valdesueiro, L. Emsley, S. Jannin, M.H. Levitt, Phys. Chem. Chem. Phys. 20 (2018) 9755–9759.
[25] M. Carravetta, M.H. Levitt, J. Am. Chem. Soc. 126 (2004) 6228–6229.
[26] G. Pileio, M.H. Levitt, J. Chem. Phys. 130 (2009) 214501.
[27] G. Pileio, J. Chem. Phys. 135 (2011) 174502.
[28] S.J. Elliott, C. Bengs, L.J. Brown, J.T. Hill-Cousins, D.J. O'Leary, G. Pileio, M.H. Levitt, J. Chem. Phys. 150 (2019) 064315.
[29] J.T. Hill-Cousins, I.-A. Pop, G. Pileio, G. Stevanato, P. Håkansson, S.S. Roy, M.H. Levitt, L.J. Brown, R.C.D. Brown, Org. Lett. 17 (2015) 2150–2153.
[30] G. Stevanato, J.T. Hill-Cousins, P. Håkansson, S.S. Roy, L.J. Brown, R.C.D. Brown, G. Pileio, M.H. Levitt, Angew. Chem. Int. Ed. 54 (2015) 3740–3743.
[31] P. Hakansson, Phys. Chem. Chem. Phys. 19 (2017) 10237–10254.

[32] J.-N. Dumez, J.T. Hill-Cousins, R.C. Brown, G. Pileio, J. Magn. Reson. 246 (2014) 27–30.
[33] G. Pileio, J.-N. Dumez, I.-A. Pop, J.T. Hill-Cousins, R.C.D. Brown, J. Magn. Reson. 252 (2015) 130–134.
[34] N. Salvi, R. Buratto, S. Ulzega, I.R. Rebollo, A. Angelini, C. Heinis, J. Am. Chem. Soc. 134 (2012) 3–6.
[35] R. Buratto, D. Mammoli, E. Chiarparin, G. Williams, G. Bodenhausen, Angew. Chem. Int. Ed. 53 (2014) 11376–11380.
[36] R. Buratto, D. Mammoli, E. Canet, G. Bodenhausen, J. Med. Chem. 59 (2016) 1960–1966.
[37] R. Buratto, A. Bornet, J. Milani, D. Mammoli, B. Vuichoud, N. Salvi, M. Singh, A. Laguerre, S. Passemard, S. Gerber-Lemaire, S. Jannin, G. Bodenhausen, Chem. Med. Chem. 9 (2014) 2509–2515.
[38] P. Saul, S. Mamone, S. Glöggler, Chem. Sci. 10 (2019) 413–417.
[39] S. Glöggler, S.J. Elliott, G. Stevanato, R.C.D. Brown, M.H. Levitt, RSC Adv. 7 (2017) 34574–34578.
[40] G. Pileio, M. Carravetta, M.H. Levitt, Proc. Natl. Acad. Sci. USA 107 (2010) 17135–17139.
[41] M.C.D. Tayler, M.H. Levitt, Phys. Chem. Chem. Phys. 13 (2011) 5556–5560.
[42] S.J. DeVience, R.L. Walsworth, M.S. Rosen, Phys. Rev. Lett. 111 (2013) 173002.
[43] R. Sarkar, P.R. Vasos, G. Bodenhausen, J. Am. Chem. Soc. 129 (2007) 328–334.
[44] T. Theis, Y. Feng, T. Wu, W.S. Warren, J. Chem. Phys. 140 (2014) 014201.
[45] A.S. Kiryutin, A.N. Pravdivtsev, A.V. Yurkovskaya, H.-M. Vieth, K.L. Ivanov, J. Chem. Phys. B 120 (2016) 11978–11986.
[46] B. Kharkov, X. Duan, J. Canary, A. Jerschow, J. Magn. Reson. 284 (2017) 1–7.
[47] G. Pileio, Prog. Nucl. Magn. Reson. Spectrosc. 98-99 (2017) 1–19.
[48] Y. Feng, R.M. Davis, W.S. Warren, Nat. Phys. 8 (2012) 831–837.
[49] Z. Zhou, K. Claytor, W.S. Warren, T. Theis, J. Magn. Reson. 263 (2016) 108–115.
[50] G. Stevanato, J. Magn. Reson. 274 (2017) 148–162.
[51] S.S. Roy, G. Stevanato, P.J. Rayner, S.B. Duckett, J. Magn. Reson. 285 (2017) 55–60.
[52] C. Bengs, M.H. Levitt, Magn. Reson. Chem. (2017) 1–41.
[53] M.C.D. Tayler, M.H. Levitt, J. Am. Chem. Soc. 135 (2013) 2120–2123.
[54] D. Mammoli, B. Vuichoud, A. Bornet, J. Milani, J.-N. Dumez, S. Jannin, G. Bodenhausen, J. Chem. Phys. B 119 (2015) 4048–4052.
[55] O.W. Sørensen, G.W. Eich, M.H. Levitt, G. Bodenhausen, R.R. Ernst, Prog. Nucl. Magn. Reson. Spectrosc. 16 (1984) 163–192.
[56] O.W. Sørensen, J. Magn. Reson. (1969) 86, 1990, 435–440.
[57] M.H. Levitt, J. Magn. Reson. 262 (2016) 91–99.
[58] W.S. Warren, E. Jenista, R.T. Branca, X. Chen, Science 323 (2009) 1711–1714.
[59] M. Singh, S. Chinthalapalli, G. Bodenhausen, Chem. Phys. Lett. 623 (2015) 113–116.
[60] M. Carravetta, M.H. Levitt, J. Chem. Phys. 122 (2005) 214505.